JOURNAL OF MATERIALS SCIENCE 28 (1993) 3809–3815

$La_2Zr_2O_7$ formed at ceramic electrode/YSZ contacts

J. A. LABRINCHA, J. R. FRADE, F. M. B. MARQUES
Departamento de Engenharia Cerâmica e do Vidro, Universidade de Aveiro, P-3800 Aveiro, Portugal

Strontium-doped $LaCoO_3$ or $LaMnO_3$ materials have been studied for use as cathodes for solid oxide fuel cells (SOFCs). This choice relies on the required properties and competitive cost. However, formation of reaction products under typical electrode-firing conditions may affect the performance of SOFCs. $La_2Zr_2O_7$ was detected at YSZ/electrode interfaces. This reaction product was synthesized from powders and characterized to obtain a better understanding of its effects on cell performance. Its structural, thermal, and electrical properties are reported.

1. Introduction

The evaluation and development of cathode materials for solid oxide fuel cells (SOFCs) has been an important subject for about 20 years. Materials with the perovskite structure are still the most promising, especially those based on $LaMnO_3$ and $LaCoO_3$, with conductivities higher than $10^4\ S\,m^{-1}$ at 1000 °C [1]. These materials also have a reputation for suitable electrocatalytic activity required for high-current applications. Strontium for lanthanum substitution has been found to improve electrode properties and electrolyte/electrode compatibility [2]. Chemical and thermal expansion compatibilities are required to ensure efficient electrode to electrolyte bonding without materials degradation, mechanical failure, or formation of unwanted reaction products. These requirements have not been easily met. Labrincha *et al.* [3] demonstrated that reaction products may occur at temperatures as low as 1100 °C, which is a typical upper limit for working temperatures.

The main reaction product formed at electrode/YSZ contacts is $La_2Zr_2O_7$ for both $LaCoO_3$- and $LaMnO_3$-based electrodes. Strontium for lanthanum substitution in electrode materials usually leads to the formation of both $La_2Zr_2O_7$ and $SrZrO_3$. Increasing strontium content hinders the formation of $La_2Zr_2O_7$, but enhances the formation of $SrZrO_3$ [3, 4].

The effects of the resistive reaction product, $La_2Zr_2O_7$, on the performance of SOFCs and other electrochemical devices may be minimized by hindering its formation, or modification of its transport properties. In fact, both strategies might correspond to a better understanding of transport properties because the kinetics of solid-state reactions is often controlled by diffusion through the reaction product layer.

Early studies of the La_2O_3–ZrO_2 system [5] suggested the formation of a pyrochlore phase $La_xZr_{1-x}O_{2-x/2}$, for about $x = 0.5$ at 1000 °C. Similar pyrochlore structures based on $A_2B_2O_7$ compounds are usually regarded as a transformation of a defect, F, fluorite structure [6]. The pyrochlore, P, structure includes an empty anion position coordinated by the smaller B atoms. On the contrary, seven anions are randomly distributed over eight sites in the corresponding defect, F, structure. It is also known that some P structures disorder above a transition temperature, which increases with increasing size of the large A atoms. Van Dijk *et al.* [6] proposed an alternative model for some pyrochlore structures based on coexisting F and P phases, to account for a variable degree of ordering. The P contribution is expected to increase with decreasing temperature, which may affect the transport mechanisms. For example, the conductivity of $La_2Zr_2O_7$ can be affected by the preparation and previous thermal history after sintering [5].

Many compounds with the pyrochlore, P, structure are ionic conductors in air, at temperatures up to about 1000 °C; this includes $Gd_2Zr_2O_7$ [6], and $Sm_2Zr_2O_7$ [7]. However, the ionic conductivity of compounds with P structure is usually lower than required for use as potential electrolytes. $La_2Zr_2O_7$ is a mixed p-type and ionic conductor in air at 1000 °C [5], and this is also the case for $Tb_2Zr_2O_{7+x}$ [6].

The ionic conductivity of some pyrochlore structures has been found to follow the equation

$$\sigma T = \sigma_0 \cdot \exp[-E_a/(RT)] \quad (1)$$

The activation energies, E_a, for ionic conduction in pyrochlore structure are usually relatively low (65–85 $kJ\,mol^{-1}$), and the pre-exponential factor, σ_0, is also low. Typical values for σ_0 in $A_2Zr_2O_7$ pyrochlores are 4×10^4, 3×10^5, and $2 \times 10^7\ S\,m^{-1}\,K^{-1}$ for A = Nd, Sm, and Gd, respectively, which corresponds to decreasing ionic size [6]. Accordingly, σ_0 is expected to be about, or smaller than $10^4\ S\,m^{-1}\,K^{-1}$ for

0022–2461

$La_2Zr_2O_7$. The relevant parameters, E_a and σ_0, increase for compounds undergoing a transformation from the pyrochlore, P, structure to a fluorite, F, structure.

2. Experimental procedure

$La_2Zr_2O_7$ and a lanthanum-deficient composition, $La_{1.9}Zr_2O_{7-y}$, were prepared by solid-state reaction, starting from ZrO_2 and La_2O_3 powders. These powders were milled together for about 2 h, with yttria partially stabilized zirconia balls, in ethanol, and pressed as pellets. The pellets were sintered in air at 1600–1650 °C for different periods of time, to obtain relative densities between 70% and 92%. Yttrium-doped $La_2Zr_2O_7$ was prepared in a similar way from commercial yttria-stabilized zirconia (8YSZ) powder and La_2O_3. These pellets were fired at 1600 °C to obtain relative densities of 71% and 82%.

X-ray diffraction was used for phase identification and structural characterization of the products. Thermal expansion coefficients were measured by dilatometric analysis from room temperature to 1000 °C. Electrical transport properties were evaluated from impedance spectroscopy measurements in air. The specimens for electrical measurements were electroded with porous platinum. The effect of oxygen partial pressure on electrical conductivity was studied by impedance measurements at 10 kHz. These measurements were carried out at temperatures from 900–1100 °C, in a special furnace with an electrochemical pump and an oxygen sensor, both connected to an oxygen pressure controller, as described elsewhere [8].

3. Results and discussion

3.1. Structure

Fig. 1 shows X-ray diffractograms for the 70% dense $La_2Zr_2O_7$, the lanthanum-deficient composition, and the yttrium-doped $La_2Zr_2O_7$, fired at 1600 °C. The stoichiometric composition shows traces of free La_2O_3, indicating that the reaction between precursors was not complete; this was found for very porous stoichiometric samples only. Well-densified stoichiometric $La_2Zr_2O_7$, lanthanum-deficient and yttrium-doped materials were found to be single-phased by X-ray diffraction (XRD), with a pyrochlore-type structure. However, SEM analysis indicated the existence of small amounts ($< 1\%$–2%) of La_2O_3 finely dispersed in all compositions. The calculated lattice parameter is 1.0794 nm for the stoichiometric composition, in agreement with previous results [5]. The theoretical density is 6.04.

X-ray diffractograms for samples quenched from temperatures in the range 500–1450 °C are similar to the patterns for slowly cooled samples without additional heat treatment. The patterns for samples heat treated in very reducing atmospheres are also similar. Therefore, structural changes are not expected in the experimental conditions used to study the transport properties of these materials, or these structures were not preserved during the cooling process.

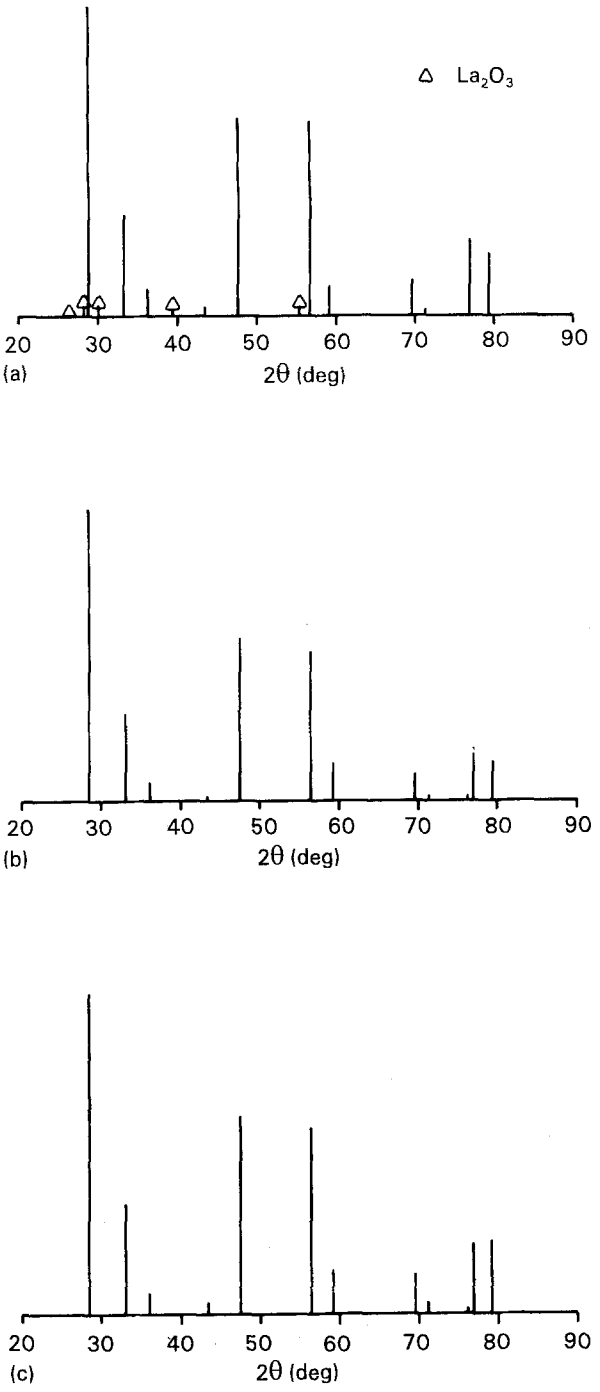

Figure 1 X-ray diffractograms for (a) undoped, (b) lanthanum-deficient and (c) yttrium-doped $La_2Zr_2O_7$ samples.

3.2. Thermal expansion behaviour

The linear thermal expansion coefficient measured for the 92% dense $La_2Zr_2O_7$ ($70 \times 10^{-7}\,°C^{-1}$) is lower than the value measured for YSZ ($96 \times 10^{-7}\,°C^{-1}$). This difference enhances the thermal expansion mismatch between YSZ electrolyte and $LaMnO_3$ (about $116 \times 10^{-7}\,°C^{-1}$), or $LaCoO_3$ ($215 \times 10^{-7}\,°C^{-1}$) electrodes. Therefore, the formation of an $La_2Zr_2O_7$ layer increases the risk of mechanical failure during thermal cycling.

3.3. Transport properties

3.3.1. Effect of oxygen partial pressure

Fig. 2 shows the effect of oxygen partial pressure on the electrical conductivity of a 70% dense stoichiometric sample, at 900 and 1000 °C. The conductivity

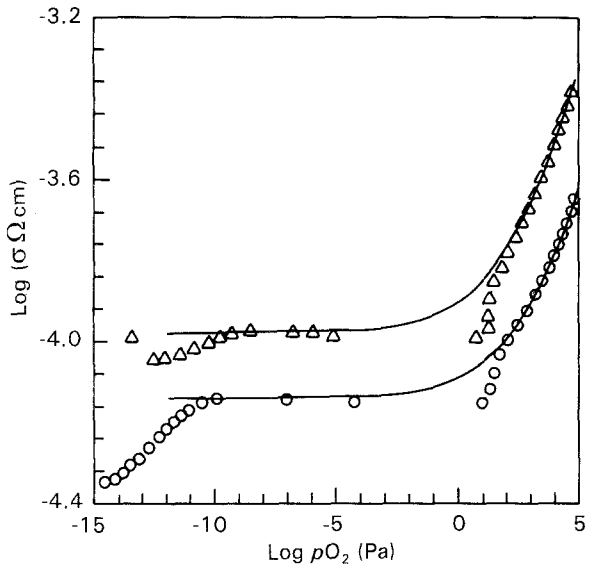

Figure 2 Effect of oxygen partial pressure on electrical conductivity of a stoichiometric $La_2Zr_2O_7$ sample at (○) 900 °C and (△) 1000 °C. (——) Obtained by fitting Equation 2 to experimental data.

was found almost independent of pO_2 in the range 10^{-10}–1 Pa; this is typical of an ionic domain. However, the oxygen sensor readings are not completely reliable in the intermediate oxygen partial pressure range for the present working conditions, and experimental data in the range 10^{-10} to ~1 Pa must be considered with caution [9, 10]. In fact, the sensor response in this range changes quickly when inert + oxygen gas mixtures are being used, and significant differences in oxygen pressure can be found between the sensor and the sample being tested [8–10]. In any circumstances, the overall small differences in conductivity observed between 1 Pa and the most extreme reducing conditions obtained in these measurements are coherent with the idea of an ionic domain observed in this region. These data also show increase in conductivity for oxygen partial pressures higher than about 1 Pa, which suggests the onset of electronic p-type conduction, as reported previously [5, 7]. However, the slope of this log(σ) versus log(pO_2) dependence remains smaller than 1/6 or 1/4 expected for typical p-type conduction in most oxides. The full lines in Fig. 2 correspond to mixed conduction, and are described by

$$\sigma = \sigma_i + \sigma_{e0} \cdot (pO_2)^{1/4} \quad (2)$$

which fits the experimental results except for very low oxygen partial pressures and for a narrow intermediate range centred at about 1 Pa. The corresponding ionic transport numbers in air, estimated from results of data fitting, decrease with increasing temperatures ($t_i = 0.4$ at 900 °C and $t_i = 0.3$ at 1000 °C).

The decrease in conductivity for pO_2 lower than about 10^{-10} Pa is poorly understood. The weak dependence shown in Fig. 2 for low oxygen partial pressures does not suggest change in defect structure. In addition, there is also no evidence of any structural transition in X-ray diffractograms of samples heat treated in reducing conditions, and then quenched to room temperatures. The decrease in conductivity is enhanced with decreasing temperatures, which might suggest defect interactions [11]. However, this explanation is unlikely for the undoped material, and defect interactions should be enhanced rather than cancelled in the yttrium-doped $La_2Zr_2O_7$ due to aliovalent Y^{3+} for Zr^{4+} substitution (Fig. 3). As a consequence, the apparent decrease in conductivity under reducing conditions is more likely to be explained by the already mentioned non-ideal response of the oxygen sensor in the intermediate oxygen pressure range rather than by the transport properties of the zirconate.

The effect of oxygen partial pressure on the conductivity of 71% dense yttrium-doped $La_2Zr_2O_7$ is shown in Fig. 3. This composition shows a larger ionic domain down to 10^{-15} Pa or smaller oxygen partial pressures, except possibly at 900 °C. The data for 900 °C were also fitted by Equation 2 (full line), which gives an ionic transport number $t_i = 0.59$ in air. The conductivity of the yttrium-doped sample is about one order of magnitude higher than for the stoichiometric sample with similar porosity.

3.3.2. Temperature dependence

Figs 4–6 show normalized impedance spectra obtained in air at temperatures from 400–1000 °C. The existence of depleted arcs corresponds to a distribution of relaxation times rather than a single process, and the angle below the real axis is a measure of that distribution. The widest distribution is for the 70% dense undoped sample (Fig. 4). On the contrary, the 82% yttrium-doped sample is close to a single process (Fig. 6). The low-temperature spectra for the 92% dense $La_2Zr_2O_7$ show the separation of high-frequency and intermediate-frequency contributions (Fig. 5). This is not the case for the 70% dense undoped sample, which has dominant intermediate frequency contributions, at least for temperatures up to 750 °C.

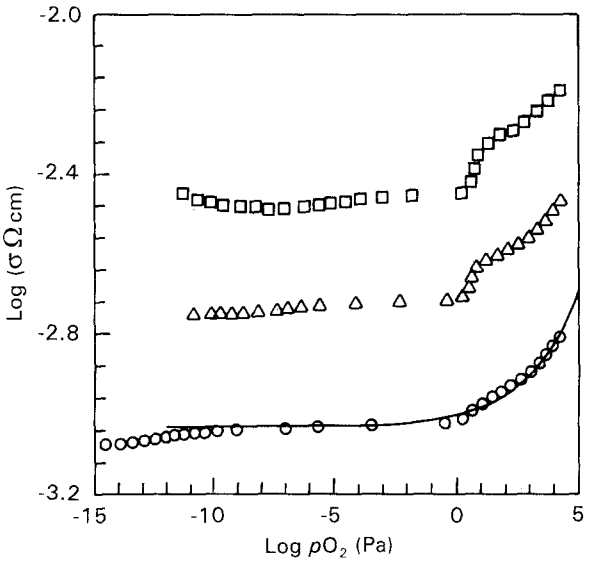

Figure 3 Effect of oxygen partial pressure on electrical conductivity of an yttrium-doped $La_2Zr_2O_7$ sample at (○) 900 °C, (△) 1000 °C and (□) 1100 °C. (——) Obtained by fitting Equation 2 to experimental data.

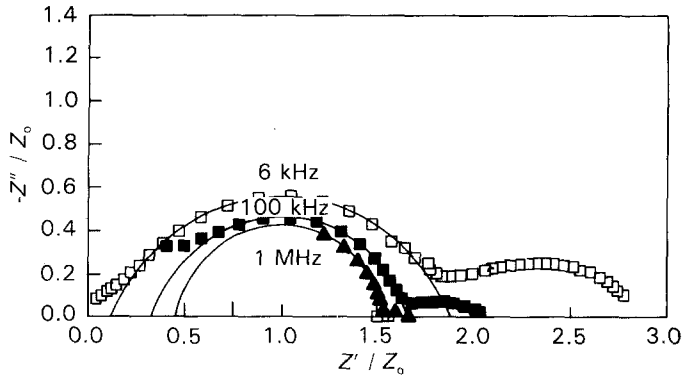

Figure 4 Normalized impedance spectra for a porous $La_2Zr_2O_7$ sample at (□) 500 °C, (■) 750 °C, and (▲) 1000 °C.

Some typical frequencies are shown in Figs 4–6 to demonstrate that similar processes are responsible for the high-frequency terms in dense undoped and yttrium-doped $La_2Zr_2O_7$. The high-frequency components are typical of bulk (intragrain) properties. In addition, the intermediate components also correspond to similar frequency for both dense and porous undoped materials. These intermediate contributions are usually related to microstructural effects or resistive grain boundaries, which is consistent with the differences in density. However, these microstructural effects cannot be related to porosity only, because yttrium for zirconium substitution contributes to eliminate these effects in the relatively porous (82% dense) yttrium-doped material.

The low-frequency arcs in Fig. 4 correspond to typical frequencies for electrode processes. Similar low-frequency arcs were found for the 92% dense sample at high temperatures. These relative contributions decrease with increasing temperature. Low electrode dispersion (especially at high temperatures) may also be considered an indication of significant electronic transport numbers [12].

The temperature dependence in air for the electrical conductivity of $La_2Zr_2O_7$ (Fig. 7) was evaluated from these impedance spectra. The conductivity of the 70% dense sample is about 2.7×10^{-2} S m^{-1} at 1000 °C, which agrees with previous results [5]. However, the conductivity of the 92% dense sample is almost one order of magnitude higher than for the previous porous sample, and the conductivity of the 82% dense yttrium-doped sample is even higher. These results are two to three orders of magnitude lower than the conductivity of YSZ (10 S m^{-1} at 1000 °C), and even lower than typical cathode materials (10^4–10^5 S m^{-1} at 1000 °C).

The Arrhenius plots in Fig. 7 show changes in slope at about 700 °C, for every sample. The activation energies are similar in the high-temperature range (98 kJ mol^{-1} for the undoped samples and 101 kJ mol^{-1} for the yttrium-doped sample) and higher than the usual values for the P-type structures. On the contrary, the low-temperature dependence is different for every sample although within a range of values nearer to those reported for similar materials [5, 6]. The low-temperature data of the 70% dense undoped sample fit an Arrhenius dependence with an activation energy

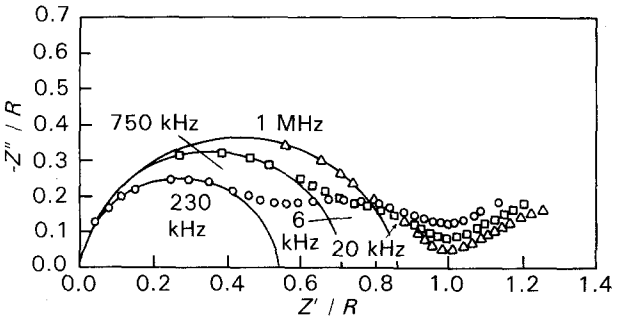

Figure 5 Normalized impedance spectra for a 92% dense $La_2Zr_2O_7$ sample at (○) 400 °C, (□) 500 °C and (△) 600 °C.

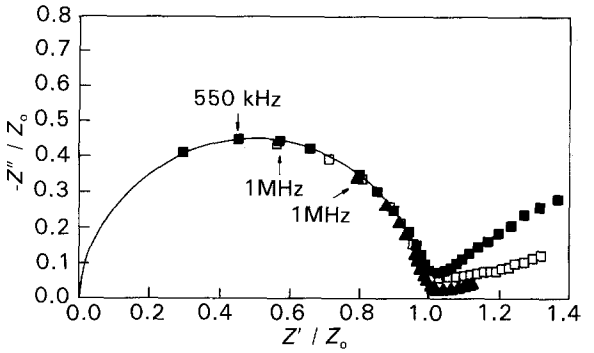

Figure 6 Normalized impedance spectra for a 82% dense yttrium-doped $La_2Zr_2O_7$ sample at (■) 400 °C, (□) 500 °C, (▲) 600 °C.

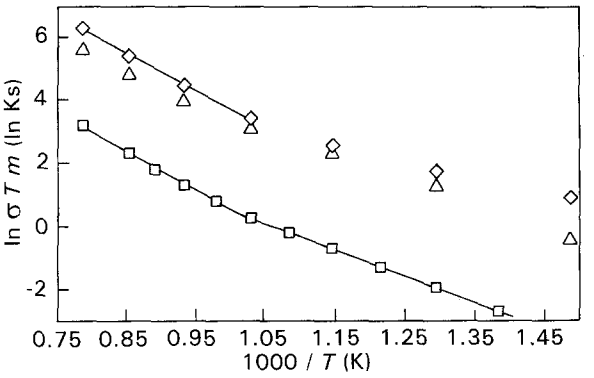

Figure 7 Temperature dependence for the electrical conductivities of (□) a 70% dense stoichiometric $La_2Zr_2O_7$ (70D) sample, (△) a 92% dense $La_2Zr_2O_7$ (92D) sample, and (◇) a 82% dense yttrium-doped sample, $La_2(Zr, Y)_2O_7$.

of 69 kJ mol^{-1}, and a pre-exponential factor $\sigma_0 = 1.33 \times 10^4\ \Omega^{-1}\,m^{-1}\,K^{-1}$ well within the expected ranges for oxygen ion conduction in a pyrochlore structure [5, 6]. However, this finding is still inconclusive because the differences in impedance spectra (Figs 4 and 5) suggest major microstructure or grain-boundary contributions.

A possible explanation for the failure of a single Arrhenius dependence including the high- and low-temperature conductivity data might be a transition between different conduction mechanisms (grain-boundary to intragrain conduction). While changes in slope observed for the 92% dense sample might be associated with this situation, it can be seen that the relative magnitude of the activation energies in both temperature ranges are contrary to this hypothesis. This cannot also explain the behaviour of the yttrium-doped sample shown in Fig. 6. A transition from ionic to electronic or mixed conduction is a possible explanation. This transition is expected to occur in the high-temperature range (700–1100 °C), with ionic transport numbers decreasing from unity to values lower than 0.5 with increasing temperature, and agrees with the effect of oxygen partial pressure (Figs 2 and 3). Finally, an order–disorder transition might also be assumed, as found for some typical F fluorite structures. Such a transition was suggested for YSZ at about 550 °C [13]. However, this was not detected by X-ray diffraction of samples quenched from temperatures in the range 500–1450 °C. The high mobility of oxygen ions in the pyrochlore structure suggests that the quenching may not be effective in preventing low-temperature ordering, in which case high-temperature X-ray diffraction could provide confirmation of structural changes.

4. Proposed defect structure

4.1. Undoped $La_2Zr_2O_7$

The ratio between large interstitial anion sites and regular anion sites is relatively high in the pyrochlore structure. Therefore, anti-Frenkel type defects are expected to dominate the defect structure, as usually found for fluorite or derived structures like the C-type cubic structure [7]. For the undoped material, and on assuming the Kroger–Vink notation

$$O_O \overset{K_1}{=} V_O^{\cdot\cdot} + O_i'' \tag{3}$$

$$O_2 \overset{K_2}{=} 2O_i'' + 4h^{\cdot} \tag{4}$$

$$O \overset{K_3}{=} e' + h^{\cdot} \tag{5}$$

where $K_3 \ll K_1$. The overall electroneutrality condition can be written

$$2[V_O^{\cdot\cdot}] + p = 2[O_i''] + n \tag{6}$$

where n and p are the concentrations of electrons and electron holes, $[V_O^{\cdot\cdot}]$ and $[O_i'']$ are the concentrations of oxygen vacancies and interstitial oxygen ions fully ionized. On assuming a traditional treatment, chemical equilibrium constants can be written for these reactions, giving the following additional relations

$$K_1 = [V_O^{\cdot\cdot}]\cdot[O_i''] \tag{7}$$

$$K_2 = [O_i'']^2\cdot p^4/pO_2 \tag{8}$$

$$K_3 = n\cdot p \tag{9}$$

The increase in electrical conductivity with oxygen partial pressure suggests an electron hole contribution for the range $pO_2 > 1$ Pa (Fig. 2). $La_2Zr_2O_7$ must be a mixed conductor in air at about 1000 °C as demonstrated by the effects of oxygen partial pressure. Therefore, the expected differences between ionic and electronic mobilities suggest that the concentration of ionic defects must be much larger than for the electronic charge carriers. Following the assumption that anti-Frenkel type defects are the dominant ionic defects, the appropriate electroneutrality condition in air is then $[V_O^{\cdot\cdot}] = [O_i'']$. The ionic conductivity in air is also expected similar to the ionic plateau in Fig. 2. On assuming an ionic to electronic mobility ratio of about 1:100, and that oxygen vacancies are the effective ionic charge carriers because of their high mobility, this gives p: $[V_O^{\cdot\cdot}] = 1.2/40$ in air at 900 °C ($t_i = 0.4$). These approximate conditions in air, ($[V_O^{\cdot\cdot}] = [O_i'']$, and p: $[V_O^{\cdot\cdot}] = 1.2/40$), were used to evaluate the ratio between equilibrium constants K_1 and K_2

$$K_2 = 4 \times 10^{-6}\, K_1^3\ \text{atm}^{-1} \tag{10}$$

In addition, the ionic plateau and conductivity changes in the low oxygen partial pressure range (Fig. 2) suggest that the electronic conductivity remains negligible down to oxygen partial pressures smaller than 10^{-14} Pa, which can be met for a ratio $K_1:K_3$ of about nine orders of magnitude. These relations between equilibrium constants K_1, K_2 and K_3 were used to solve Equations 6–9, and evaluate the oxygen pressure dependence of defect concentrations indicated in the Brouwer-type diagram shown in Fig. 8. As none of these concentrations is, in fact, known, the concentration scale is expressed in arbitrary units. This defect diagram also gives the full line shown in Fig. 2 (for 900 °C), on assuming that the oxygen vacancies are the ionic charge carriers, and for the previously assumed electronic to ionic mobility ratio 100:1. Because the actual mobilities and defect concentrations are unknown, a mobility factor, $f_{\mu i}$, was evaluated to match these concentrations of oxygen vacancies and the ionic conductivity in the ionic plateau. The corresponding electronic conduction was

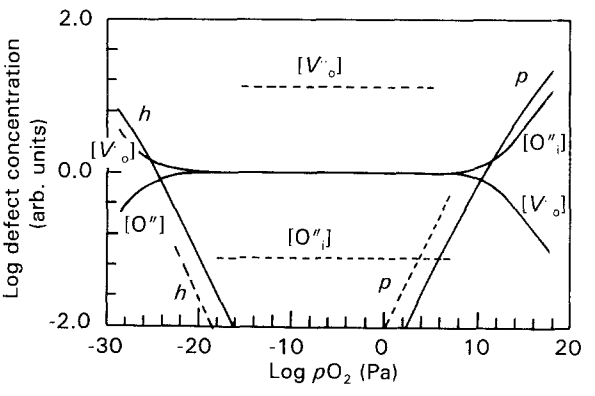

Figure 8 Normalized defect diagrams predicted for (——) undoped and (– – –) yttrium-doped $La_2Zr_2O_7$ compositions.

computed in the same manner based on the assumed differences in mobility of defects.

The major shortcoming of the proposed defect diagram is the failure to explain the drop in conductivity found for the undoped material at low oxygen partial pressures, which contradicts the defect diagram shown in Fig. 8. Similar contradictions between the expected increase in charge carrier concentrations and decrease in conductivity have been found in different materials [14]; this is usually attributed to defect interactions or association, which is unlikely for undoped $La_2Zr_2O_7$, as already mentioned.

4.2. Yttrium-doped $La_2Zr_2O_7$

The similar behaviour observed for the temperature and oxygen partial pressure dependence of undoped and yttrium-doped $La_2Zr_2O_7$ suggests that the predominant charge transport mechanisms are similar but different concentrations of charge carriers are present in each case. Additional evidence for this assumption is provided by the similarity between the typical frequencies shown in Figs 5 and 6, corresponding to the bulk impedance arcs. Therefore, the increase in conductivity and ionic transport numbers in yttrium-doped sample (Figs 2 and 3), are consistent with the following mechanism

$$Y_2O_3 + La_2O_3 \xrightarrow{La_2Zr_2O_7} 2Y'_{Zr} + 2La_{La} + 6O_O + V_O^{\cdot\cdot} \quad (11)$$

which enhances the concentration of oxygen vacancies. Whether or not all yttrium ions occupy zirconium positions is not clear but the observed increase in ionic domain is coherent with this assumption. Equation 3 also predicts a decrease in concentration of interstitial oxygen ions, which confirms that oxygen vacancies must be the main ionic charge carriers. In this case, the electroneutrality condition must include the concentration $[Y'_{Zr}]$, and the concentration of oxygen vacancies are primarily determined by the concentration of yttrium ions. For 16% Y for zirconium substitution, the concentration $[Y'_{Zr}]$ is about $0.16 \times 2/7 = 0.0457$ per anion position. Defect interactions or association of positive and negative defects is expected for high defect concentrations, and the concentration of effective ionic charge carriers may be much smaller than expected from yttrium for zirconium contents. The mechanisms of defect interactions and the relevant equilibrium constants are not known, which prevents a prediction of a complete defect diagram.

Nevertheless, the ionic conductivity increases by a factor of about 13 at 900 °C, in the ionic plateau (Figs 2 and 3). A similar increase in concentration of effective ionic charge carriers can be expected, which gives

$$[V_O^{\cdot\cdot}] = 13[V_O^{\cdot\cdot}]_{und} = 13\,K_1^{1/2} \quad (12)$$

A defect diagram for the present conditions can also be drawn based on the previous assumptions (Fig. 8). The equilibrium constants K_1, K_2, and K_3 were assumed to be similar for both the undoped and yttrium-doped materials, on the basis of similar structures. Therefore,

$$[O_i''] = K_1/[V_O^{\cdot\cdot}] = 0.077\,K_1^{1/2} \quad (13)$$

The concentrations of electronic defects were obtained from the corresponding equations already presented. The partial defect diagram obtained in this manner is shown dashed in Fig. 8. This partial diagram is expected as long as the concentrations of electronic defects remain much lower than $[V_O^{\cdot\cdot}]$. The electroneutrality is ensured by Y'_{Zr}, and possibly also charged associates, $(Y'_{Zr}V_O^{\cdot\cdot})$. This partial defect diagram also gives the full line in Fig. 3, for an electronic to ionic mobility ratio of about 180:1; this is close to the corresponding ratio assumed to fit the conductivity data for the undoped material. The deviations at low oxygen partial pressures (below $\approx 10^{-10}$ Pa), are much smaller than for the undoped material.

5. Conclusions

$La_2Zr_2O_7$ and yttrium-doped $La_2Zr_2O_7$ are mixed conductors in air at temperatures of about 900–1100° C, and pure ionic conductors under moderately reducing conditions. The conduction mechanisms are similar for undoped or yttrium-doped materials, except for the increase in concentration of charge carriers for the yttrium-doped material, and correspondingly higher ionic transport numbers. Differences in activation energy for electrical conductivity above and below 700 °C can be interpreted as a result of an increasingly important electronic conductivity contribution with temperature or an order–disorder type transformation. Further work is required to study the drop in conductivity at low oxygen partial pressures.

Both undoped and yttrium-doped $La_2Zr_2O_7$ have much lower electrical conductivities than YSZ or typical cathode materials, which is detrimental for electrode processes. However, mixed conduction in a compact lanthanum zirconate layer formed at the interface between YSZ and the cathode material is probably less severe than for a material with a similar pure electronic or ionic conductivity. A lanthanum zirconate layer also increases the thermal expansion mismatch between YSZ and $LaMnO_3$- or $LaCoO_3$-based cathodes.

The transport properties of lanthanum zirconate show that its high-temperature formation at the interface YSZ/cathode is unlikely to be kinetically hindered by slow diffusion of oxygen ions through that layer.

Acknowledgements

This work was performed with financial support from JNICT and INIC (Portugal).

References

1. Y. TAKEDA, R. KANNO, M. NODA, Y. TOMIDA and O. YAMAMOTO, *J. Electrochem. Soc.* **134** (1987) 2656.
2. A. HAMMOUCHE, E. SIEBERT and A. HAMMOU, *Mater. Res. Bull.* **24** (1989) 367.

3. J. A. LABRINCHA, J. R. FRADE and F. M. B. MARQUES, in "Proceedings of the 2nd International Symposium on SOFCs", Athens, July 1991, edited by F. Gross, P. Zegers, S. Singhal and O. Yamamoto (Common European Community, Brussels, 1991) p. 689.
4. H. YOKOKAWA, N. SAKAI, T. KAWADA and M. DOKIYA, *Solid State Ionics* **40/41** (1990) 398.
5. T. H. ETSELL and S. N. FLENGAS, *Chem. Rev.* **70** (1970) 339.
6. M. P. VAN DIJK, K. J. de VRIES and A. J. BURGGRAAF, *Solid State Ionics* **9/10** (1983) 913.
7. K. SHINOZAKI, *J. Amer. Ceram. Soc.* **62** (1979) 538.
8. F. M. B. MARQUES and G. P. WIRTZ, *ibid.* **74** (1991) 598.
9. *Idem., ibid.*, in press.
10. G. P. WIRTZ and F. M. B. MARQUES, *ibid.*, in press.
11. J. C. C. ABRANTES, J. A. LABRINCHA, F. M. B. MARQUES and J. R. FRADE, in "Ceramics Today – Tomorrow's Ceramics", Part C, edited by P. Vincenzini (Elsevier Science, Amsterdam, 1991) p. 2265.
12. F. BEECH, W. M. JORDAN, C. R. A. CATLOW, A. SANTORO and B. C. H. STEELE, *J. Solid State Chem.* **77** (1988) 322.
13. S. P. S. BADWALL, *J. Mater. Sci.* **19** (1984) 1767.
14. J. M. DIXON, L. D. LAGRANGE, U. MERTEN, C. F. MILLER and J. T. PORTER II, *J. Electrochem. Soc.* **110** (1963) 276.

Received 7 February
and accepted 19 November 1992